INSTITUTE OF PHYSICS PUBLISHING SUPERCONDUCTOR SCIENCE AND TECHNOLOGY

Supercond. Sci. Technol. **17** (2004) 278–286 PII: S0953-2048(04)68338-2

Very high upper critical fields in MgB_2 produced by selective tuning of impurity scattering

A Gurevich[1], S Patnaik[1,5], V Braccini[1,3], K H Kim[2], C Mielke[2], X Song[1], L D Cooley[1,6], S D Bu[1], D M Kim[1], J H Choi[1], L J Belenky[1], J Giencke[1], M K Lee[1], W Tian[4], X Q Pan[4], A Siri[3], E E Hellstrom[1], C B Eom[1] and D C Larbalestier[1]

[1] Applied Superconductivity Center, Department of Materials Science and Engineering, and Department of Physics, University of Wisconsin, Madison, WI 43706, USA
[2] National High Magnetic Field Laboratory, Los Alamos National Laboratory, Los Alamos, NM 87545, USA
[3] Department of Physics, University of Genova, INFM-LAMIA, Via Dodecaneso 33, 16146 Genova, Italy
[4] Department of Materials Science and Engineering, University of Michigan, Ann Arbor, MI 48109, USA

Received 28 August 2003, in final form 19 November 2003
Published 19 December 2003
Online at stacks.iop.org/SUST/17/278 (DOI: 10.1088/0953-2048/17/2/008)

Abstract

We report a significant enhancement of the upper critical field H_{c2} of different MgB_2 samples alloyed with nonmagnetic impurities. By studying films and bulk polycrystals with different resistivities ρ, we show a clear trend of an increase in H_{c2} as ρ increases. One particular high resistivity film had a zero-temperature $H_{c2}(0)$ well above the H_{c2} values of competing non-cuprate superconductors such as Nb_3Sn and Nb–Ti. Our high-field transport measurements give record values $H_{c2}^{\perp}(0) \approx 34$ T and $H_{c2}^{||}(0) \approx 49$ T for high resistivity films and $H_{c2}(0) \approx 29$ T for untextured bulk polycrystals. The highest H_{c2} film also exhibits a significant upward curvature of $H_{c2}(T)$ and a temperature dependence of the anisotropy parameter $\gamma(T) = H_{c2}^{||}/H_{c2}^{\perp}$ opposite to that of single crystals: $\gamma(T)$ *decreases* as the temperature decreases, from $\gamma(T_c) \approx 2$ to $\gamma(0) \approx 1.5$. This remarkable H_{c2} enhancement and its anomalous temperature dependence are a consequence of the two-gap superconductivity in MgB_2, which offers special opportunities for further H_{c2} increases by tuning of the impurity scattering by selective alloying on Mg and B sites. Our experimental results can be explained by a theory of two-gap superconductivity in the dirty limit. The very high values of $H_{c2}(T)$ observed suggest that MgB_2 can be made into a versatile, competitive high-field superconductor.

1. Introduction

Since the discovery of the 'intermediate-T_c' superconductor MgB_2 with a critical temperature T_c of 39 K [1, 2], many efforts have been made to increase the ability of MgB_2 to sustain superconductivity at higher magnetic fields. This problem is of fundamental interest and is vital for applications because MgB_2 exhibits high critical current densities J_c [3–6], no intrinsic current blockage by grain boundaries [7] and comparatively weak anisotropy and thermal fluctuations. Yet, clean MgB_2 has so far offered no clear advantages compared to existing practical high-field superconductors because of

[5] Present address: School of Physical Sciences, Jawaharlal Nehru University, New Delhi 110067, India.
[6] Present address: Department of Materials Science, Brookhaven National Laboratory, Upton, NY 11973, USA.

the rather low upper critical fields, $H_{c2}^{\perp}(0) \approx 3.5$ T and $H_{c2}^{||}(0) \approx 18$ T perpendicular and parallel to the *ab* plane of MgB_2 single crystals, respectively [8–12]. Indeed, the key to magnet applications of superconductors lies in the rare combination of low cost and a ready wire fabrication route, which produces conductors with high upper critical fields H_{c2} and critical current densities J_c [13]. Modern conductors are made from Nb–Ti ($T_c = 9$ K, H_{c2} (4.2 K) $= 10$ T), Nb_3Sn ($T_c = 18$ K, H_{c2} (4.2 K) $= 28$ T) and the high-temperature superconductors (HTS), $Bi_2Sr_2CaCu_2O_{8-x}$ ($T_c \sim 90$ K) and $(Bi, Pb)_2Sr_2Ca_2Cu_3O_{10-x}$ ($T_c \sim 110$ K). At low temperatures the HTS polycrystals have H_{c2} well above 50 T, but they suffer from strong current relaxation, high anisotropy ($H_{c2}^{||}/H_{c2}^{\perp} > 20$) and weak-linked grain boundaries that obstruct the current except when crystallographically textured. Because of their large H_{c2} anisotropy, HTS conductors must be made in tape form, whereas isotropic Nb-based superconductors are easily fabricated into round wires capable of generating magnetic fields above 20 T, but only at $T = 2$–5 K. However, due to recent advances in cryocoolers, many electric utility, fusion and high-energy physics applications may be best optimized at temperatures of 10–35 K [14], a domain for which MgB_2 could provide the cheapest superconducting wires [15]. It is the low upper critical field which has mainly limited the potential applications of clean MgB_2, for which H_{c2} (4.2 K) is even less than that of Nb–Ti. Here we show how $H_{c2}(T)$ of MgB_2 can be radically enhanced beyond that of any Nb-based superconductor by introducing strong impurity scattering. The resulting increase of H_{c2}, along with the significant decrease in H_{c2} anisotropy, from $H_{c2}^{||}/H_{c2}^{\perp} \approx 5$–6 [2] down to $H_{c2}^{||}/H_{c2}^{\perp} < 2$, can make MgB_2 well suited for high-field magnet applications at 20–30 K where HTS conductors presently are without challenge [13].

We show that a significant portion of the anomalous increase in H_{c2} results from the two-gap superconductivity in MgB_2, which has been well established by many *ab initio* calculations [16, 17], STM experiments [18], point contact [19] and Raman [20] spectroscopy, specific heat [21] and neutron diffraction [22] measurements. As a result, there is compelling evidence that MgB_2 is the first superconductor with two weakly coupled superconducting gaps Δ_σ (4.2 K) ≈ 7.2 meV and Δ_π (4.2 K) ≈ 2.3 meV. These gaps reside on different disconnected sheets of the Fermi surface, which is comprised of nearly cylindrical parts formed by *in-plane* σ antibonding p_{xy} orbitals of B and a more isotropic tubular network formed by *out-of-plane* π bonding and antibonding p_z orbitals of B. Such a Fermi surface gives rise to three different impurity scattering channels in MgB_2 alloys: intraband scattering within each σ and π sheet and interband scattering between them [23]. It is these multiple scattering channels which make it possible to increase H_{c2} of MgB_2 to a much greater extent than in one-gap superconductors, not only by the usual increase of the normal state resistivity ρ, as in low-T_c superconductors [24–26], but also by optimizing the relative weight of the σ and π scattering rates by selective substitution of boron or magnesium.

In low-T_c s-wave superconductors, alloying with nonmagnetic impurities does not affect T_c much but does increase the slope $H'_{c2} = |dH_{c2}/dT|$ at T_c proportionally to the residual resistivity ρ. This behaviour is characteristic of the dirty limit $\hbar v_F \gg 2\pi l k_B T_c$, where l is the electron mean free path, v_F is the Fermi velocity and $\hbar$ and k_B are the Planck and Boltzmann constants, respectively. The zero-temperature field $H_{c2}(0)$ is then given by [26]

$$H_{c2}(0) = 0.69 T_c H'_{c2}(T_c). \quad (1)$$

Because $H_{c2}(0)$ increases proportionally to ρ, alloying is a well-established route to H_{c2} enhancement in Nb–Ti [24] and the A15 compounds [25]. The same approach has been successfully applied to MgB_2 as well, which was demonstrated by the alloying of MgB_2 films [27], bulk samples [28], and also by proton [29] and neutron [30] irradiation of polycrystalline MgB_2. In what follows we show, both experimentally and theoretically, that because of the two-gap superconductivity in MgB_2, equation (1) in fact strongly *underestimates* the actual $H_{c2}(0)$ of dirty MgB_2.

2. Experimental details

To show how far H_{c2} can actually be increased by alloying, we performed high-field transport measurements on samples of very different purities: a fibre-textured, high-resistivity ($\rho(40\ \text{K}) = 220\ \mu\Omega$ cm) *c*-axis-oriented film on a (111) $SrTiO_3$ substrate [31], a low-resistivity ($\rho(40\ \text{K}) = 7\ \mu\Omega$ cm), *c*-axis-oriented, epitaxial MgB_2 film on a (0001) Al_2O_3 substrate [32] and three untextured polycrystalline bulk MgB_2 samples of different resistivities, $\rho(40\ \text{K}) =$ 1–18 $\mu\Omega$ cm [33]. The 220 $\mu\Omega$ cm, pulsed laser deposited film was earlier reported to have a macroscopically inhomogeneous resistivity $\rho(40\ \text{K}) \approx 360$–$440\ \mu\Omega$ cm [27, 31], but subsequent transmission electron microscopy [34] showed that approximately half of the measured film thickness was fully reacted MgB_2. The film had $T_c \sim 31$ K and extremely high resistivity compared to the nominal $\rho(40\ \text{K}) \approx 1\ \mu\Omega$ cm of 'clean' MgB_2 [12]. The sputtered epitaxial film [32] has 400 nm thickness of MgB_2, $T_c = 35$ K and much lower $\rho(40\ \text{K}) \approx 7\ \mu\Omega$ cm. The bulk samples have $\rho(40\ \text{K}) =$ $1\ \mu\Omega$ cm as produced by direct reaction, but 18 $\mu\Omega$ cm after subsequently heating in Mg vapour followed by slow cooling [33]. After ageing for two months, the resistivity ρ (40 K) for this sample fell from 18 down to 5 $\mu\Omega$ cm.

Measurements of $H_{c2}(T)$ on thin films were made partly in DC fields up to 14 T in a quantum design physical property measurement system (PPMS) and partly in the high-field facility at LANL capable of generating 32 ms asymmetric field pulses up to 50 T. A combination of an ultrafast digitizer and a lock-in amplifier enabled us to take over 32 000 data points of the measured 100 kHz signal during the pulse, from T_c to 1.4 K with ~10 mK sensitivity. Three data sets taken for the films gave consistent results. The greater cross section ~0.5 mm × 0.5 mm and lower ρ of the bulk samples made the resistive transitions under pulsed fields so noisy that we had to measure them under dc conditions. DC measurements up to 14 T were performed in the PPMS while high field resistance $R(B)$ measurements were made in the 33 T resistive magnet at the NHMFL in Tallahassee, FL on the sample annealled in Mg vapour after it was aged for two months.

Figures 1(a) and (b) show the resistive transitions from 1.5 to 30 K of the 220 $\mu\Omega$ cm film as a function of pulsed magnetic fields for perpendicular and parallel fields. These transitions

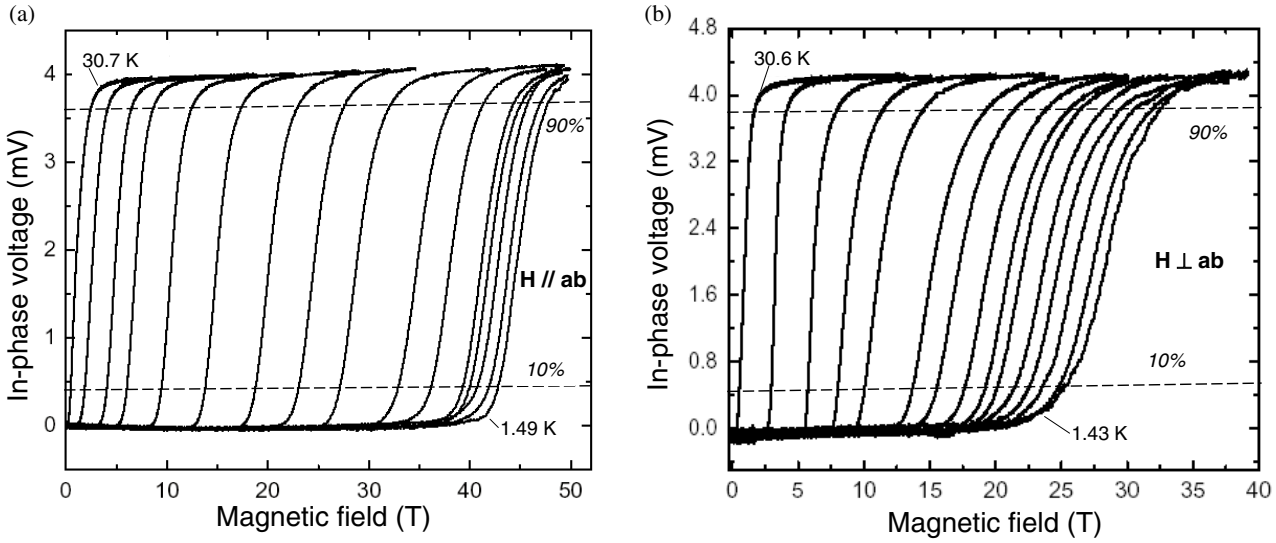

Figure 1. Resistive transitions taken at the LANL pulsed field facility on the high resistivity ($\rho(40\ \mathrm{K}) = 220\ \mu\Omega$ cm) film. Data were taken for several runs on more than one occasion. The horizontal broken lines correspond to $0.1R(T_c)$ and $0.9R(T_c)$, defining the irreversibility and the upper critical fields plotted in figure 2. (a) Data taken at temperatures of 1.43, 2.12, 2.71, 4.06, 4.5, 5.1, 5.95, 8.11, 11.4, 13.95, 17.1, 20.05, 24, 28 and 30.6 K for a field applied perpendicular to the film and to the *ab* plane. (b) Data taken at temperatures of 1.49, 1.99, 2.7, 3.76, 4.41, 7.13, 10.11, 13.33, 15.99, 18.64, 21.8, 24.8, 27.03, 28.85, 29.9 and 30.7 K for a field applied parallel to the film and to the *ab* plane.

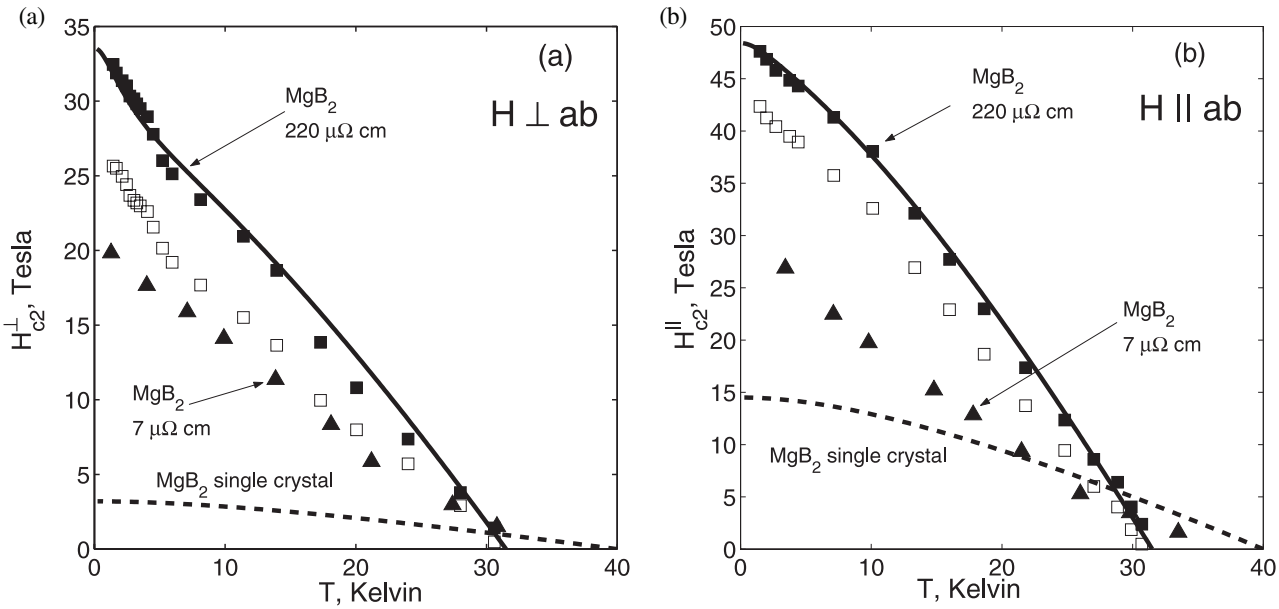

Figure 2. The upper critical fields $H_{c2}(T)$ (full squares) and irreversibility fields $H^*(T)$ (open squares) for a high resistivity 220 $\mu\Omega$ cm film, and $H_{c2}(T)$ for a low resistivity 7 $\mu\Omega$ cm film (full triangles). Full curves show $H_{c2}(T)$ calculated from equation (2) with the coupling constants $\lambda_{\sigma\sigma} = 0.81$, $\lambda_{\pi\pi} = 0.28$, $\lambda_{\sigma\pi} = 0.115$ and $\lambda_{\pi\sigma} = 0.09$ [38]. (a) Corresponds to $\mathbf{H} \perp ab$, for which the theoretical curve is plotted for $D_\pi = 0.12D_\sigma$. (b) Corresponds to $\mathbf{H} \parallel ab$, for which the theoretical curve is plotted for $[D_\pi^{(c)} D_\pi^{(ab)}]^{1/2} = 0.2[D_\sigma^{(c)} D_\sigma^{(ab)}]^{1/2}$. The broken curves show $H_{c2}(T)$ plotted for MgB_2 single crystals [11].

agree well with our earlier DC measurements up to 9 T from another piece of this same film for which we defined the effective irreversibility field $H^*(T)$ as $R(H^*) = 0.1R(T_c)$ and the upper critical field as $R(H_{c2}) = 0.9R(T_c)$ [27]. We use here a more conservative criterion for H_{c2} in figure 1 than the usual definition for H_{c2} as the onset of the resistive transitions, which are much narrower ($H^*(T) \sim 0.8$–$0.9H_{c2}(T)$) compared to those observed on high-T_c cuprates [35]. Although our definition underestimates the actual upper critical field (as seen from figure 1, the field differences between the onset and the $0.9R(T_c)$ point can be as high as 3–4 T), it makes it less sensitive to noise on the upper parts of the $R(H)$ curves.

$H_{c2}^{||}(T)$ and $H_{c2}^{\perp}(T)$ curves for the two films are shown in figure 2, from which it is immediately clear that the temperature dependence of $H_{c2}(T)$ is rather anomalous. Indeed, equation (1) would predict $H_{c2}^{\perp}(0) \approx 10.5$ T for the cleaner film, while in fact it exceeds 20 T. In the parallel configuration, equation (1) gives $H_{c2}^{||}(0) \approx 20$ T versus the

measured 30 T. Even more striking is the behaviour of the dirtier film. Record high values of $H_{c2}^{\perp}(0) \approx 34$ T and $H_{c2}^{||}(0) \approx 49$ T are attained, both considerably exceeding the earlier low-field extrapolations of 20 and 39 T based on measurements close to T_c and the use of equation (1) [27]. Both parallel and perpendicular $H_{c2}(T)$ curves exhibit *upward* curvature and different shapes of $H_{c2}(T)$ curves for parallel and perpendicular field orientations, neither being consistent with the one-gap theory [26]. We also show the field at which $R(H) = 0.1R(T_c)$ to emphasize that the extreme high field performance capability of dirtier MgB_2 is not very sensitive to the particular definition of H_{c2}. Moreover, for $H \parallel ab$, H_{c2} of the dirty MgB_2 significantly exceeds H_{c2} of the best Nb_3Sn at all temperatures. Even for the perpendicular field ($H \perp ab$), not only is $H_{c2}(T)$ of MgB_2 still superior to Nb_3Sn, but dirty MgB_2 has essentially the same $H_{c2} = 12$ T at 20 K as the best Nb–Ti at 4.2 K.

Figure 3 collects the data for bulk, untextured MgB_2 and again shows the decisive influence of resistivity. The low-resistivity ($\rho(40\text{ K}) \approx 1\ \mu\Omega$ cm) sample has an extrapolated $H_{c2}(0) \sim 17$ T, close to that of other clean limit samples [12]. After exposure to Mg, the resistivity $\rho(40\text{ K})$ rose to 18 $\mu\Omega$ cm and $H'_{c2} = 1.2\text{ T K}^{-1}$ at 25–30 K became almost as high as H'_{c2} for a 220 $\mu\Omega$ cm film in a perpendicular field. H_{c2} then reached 9 T at 27 K, comparable to the film value in a parallel field. After re-measuring this sample about two months later, it had apparently aged, as shown by a reduced $\rho = 5\ \mu\Omega$ cm, a decreased $H_{c2}(T)$ and an increased T_c from 36.9 to 37.7 K. This ageing may result from the relaxation of stress in the quenched crystalline structure. In any case, the $H_{c2}(T)$ data show the same qualitative trends as the film data in figure 2: as the resistivity increases from 1 to 5 $\mu\Omega$ cm, $H_{c2}(0)$ approximately doubles, reaching ~29 T, close to the best $H_{c2}(0)$ value of Nb_3Sn. We do note that the interpretation of resistive transitions for polycrystals may be complicated by the percolative effects due to the anisotropy of H_{c2}, which results in different resistive transitions for crystallites with varying orientations with respect to the applied field.

The totality of the data presented in figures 2 and 3 unambiguously indicates that impurity scattering can markedly enhance H_{c2} of MgB_2 while only weakly reducing T_c. For example, as $\rho(40\text{ K})$ is increased from ~1 to ~220 $\mu\Omega$ cm, the perpendicular field $H_{c2}^{\perp}(0)$ rises nearly 10-fold, from the typical single-crystal values of ≈3–5 to ~35–39 T. However this H_{c2} enhancement is not entirely determined by the resistivity, as in dirty one-gap superconductors. As follows from figure 2, a significant portion of the H_{c2} increase comes from the anomalous low temperature upward curvature of $H_{c2}(T)$.

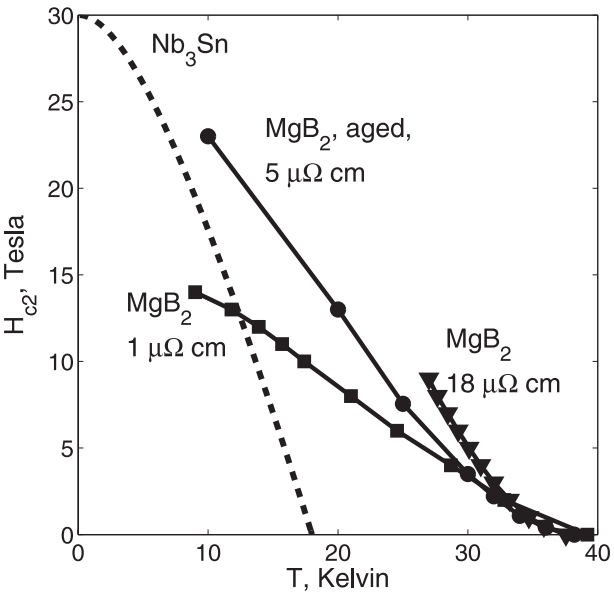

Figure 3. DC resistive transitions at a measuring current density ~1 A cm^{-2} on bulk samples: the clean one ($\rho(40\text{ K}) = 1\ \mu\Omega$ cm, full squares), the sample heated in Mg vapour and then slow-cooled ($\rho(40\text{ K}) = 18\ \mu\Omega$ cm, full diamonds) and the same sample (aged to $\rho = 5\ \mu\Omega$ cm, full circles) measured at the NHMFL two months later. In any case, $H_{c2}(T)$ significantly increases as the resistivity increases, the slope $H'_{c2} = 1.2\text{ T K}^{-1}$ at 25–30 K for the 18 $\mu\Omega$ cm sample being almost as high as H'_{c2} for the 220 $\mu\Omega$ cm film at $\mathbf{H} \perp ab$ in figure 2(a). The broken curve shows $H_{c2}(T)$ for Nb_3Sn.

3. Discussion

3.1. Two-gap, dirty-limit theory

To address the physics behind the observed anomalous behaviour of $H_{c2}(T)$, we applied a dirty-limit two-gap superconductivity theory based on the Usadel equations [36, 37] to MgB_2. In this approach the details of the complex Fermi surface of MgB_2 are not essential for calculation of H_{c2}, while the impurity scattering is accounted for by the normal state electronic diffusivity tensors $D_\sigma^{\alpha\beta}$ and $D_\pi^{\alpha\beta}$, controlled by their respective intraband scattering rates in the σ and π bands, $\Gamma_{\sigma\sigma}$ and $\Gamma_{\pi\pi}$, and interband scattering rates $\Gamma_{\pi\sigma}$ and $\Gamma_{\sigma\pi}$. For MgB_2, the interband scattering (responsible for T_c suppression by nonmagnetic impurities) is weak [23], so we assume for simplicity that $\Gamma_{\pi\sigma} = \Gamma_{\sigma\pi} = 0$ (a more general case of finite $\Gamma_{\pi\sigma}$ and $\Gamma_{\sigma\pi}$ was considered in [36]). In that case the solution of the linearized two-gap Usadel equations for $H \perp ab$ and $\Gamma_{\pi\sigma} = \Gamma_{\sigma\pi} = 0$ gives the following equation for $H_{c2}^{\perp}$ [36, 37]:

$$2w[\ln t + u(b/t)][\ln t + u(\eta b/t)] + \lambda_2[\ln t + u(\eta b/t)] + \lambda_1[\ln t + u(b/t)] = 0. \quad (2)$$

Here $t = T/T_c$, $u(x) = \psi(1/2 + x) - \psi(1/2)$, $\psi(x)$ is the Euler digamma function, $b = \hbar H_{c2} D_\sigma / 2\phi_0 k_B T_c$, ϕ_0 is the magnetic flux quantum, $\eta = D_\pi/D_\sigma$, $w = \lambda_{\sigma\sigma}\lambda_{\pi\pi} - \lambda_{\sigma\pi}\lambda_{\pi\sigma}$, $\lambda_{1,2} = \lambda_0 \pm \lambda_-$, $\lambda_0 = (\lambda_-^2 + 4\lambda_{\sigma\pi}\lambda_{\pi\sigma})^{1/2}$, $\lambda_- = \lambda_{\sigma\sigma} - \lambda_{\pi\pi}$ and the 2×2 matrix of the BCS superconducting coupling constants $\lambda_{mn} = \lambda_{mn}^{(ep)} - \mu_{mn}$ contains both the electron–phonon constants $\lambda_{mn}^{(ep)}$ and the Coulomb pseudopotential μ_{mn}. First-principles calculations of the intraband (m = n) and interband (m ≠ n) matrix elements λ_{mn} for MgB_2 gave $\lambda_{\sigma\sigma} = 0.81$, $\lambda_{\pi\pi} = 0.28$, $\lambda_{\sigma\pi} = 0.115$ and $\lambda_{\pi\sigma} = 0.09$ [38].

The $H_{c2}(T)$ curves calculated from equation (2) evolve from the classic dirty-limit, one-band BCS behaviour [26] at $D_\pi = D_\sigma$ to the rather different $H_{c2}(T)$ curves which have portions with both upward and downward curvatures for either $D_\pi \ll D_\sigma$ and $D_\pi \gg D_\sigma$ [36]. As a result, $H_{c2}(0)$ can be significantly higher than suggested by conventional extrapolation (1). To show how this happens, we first obtain $H_{c2}(T)$ near T_c by expanding equation (2) using $u(b) \approx \pi^2 b/2$ at $b \ll 1$:

$$H_{c2}^{\perp}(T) = \frac{8\phi_0\lambda_0 k_B(T_c - T)}{\hbar\pi^2(\lambda_1 D_\sigma + \lambda_2 D_\pi)}. \quad (3)$$

For the characteristic λ_{mn} values of MgB_2, but very different D_π and D_σ, the upper critical field is therefore determined by the maximum intraband diffusivity, for example, by D_π if disorder mostly causes scattering in the 'strong' σ band. The zero-temperature value $H_{c2}(0)$ is obtained using the limiting behaviour of $u(b/t) = \ln(4\gamma b/t)$ for $t \ll 1$ where $\ln\gamma = -0.577$. Then equation (3) reduces to a quadratic equation for $\ln H_{c2}$, whence

$$H_{c2} = \frac{\phi_0 k_B T_c}{2\gamma\hbar\sqrt{D_\pi D_\sigma}} \exp(g), \tag{4}$$

where $2g = [(\lambda_0/w)^2 + \ln^2\eta + 2\ln(\eta)\lambda_-/w]^{1/2} - \lambda_0/w$. For very different diffusivities, equation (4) yields $H_{c2}(0) \approx \phi_0 k_B T_c \exp(-\lambda_2/2w)/2\gamma\hbar D_\sigma$ if $D_\sigma \ll D_\pi$, but $H_{c2}(0) \approx \phi_0 k_B T_c \exp(-\lambda_1/2w)/2\gamma\hbar D_\pi$ if $D_\pi \ll D_\sigma$, so $H_{c2}(0)$ diverges as either D_σ or D_π goes to zero. Thus, unlike the region $T \approx T_c$, where $H_{c2}(T)$ is determined by the *maximum* diffusivity between D_σ and D_π, the zero-temperature $H_{c2}(0)$ is controlled by the *minimum* diffusivity. It is this feature of two-gap superconductivity which causes both the upward curvature of $H_{c2}(T)$ and the violation of equation (1) for $D_\pi \neq D_\sigma$. Equation (2) can be generalized to an arbitrary field orientation by replacing both intraband diffusivities D_m with the angular dependent effective diffusivities [36]:

$$D_m(\theta) = (D_m^{(ab)2}\cos^2\theta + D_m^{(c)}D_m^{(ab)}\sin^2\theta)^{1/2}, \tag{5}$$

where θ is the angle between **H** and the c axis, $m = (\sigma, \pi)$ and the superscripts (ab) and (c) indicate the diffusivities along the ab plane and the c axis, respectively. Equations (2) and (5) enable us to address the observed anomalous temperature dependence of the anisotropy of $H_{c2}(\theta)$ [8–12], as described in detail elsewhere [36]. Here we only use the fact that, for the parallel field orientation, $\mathbf{H} \parallel ab$, the effective diffusivities in equations (2)–(4) become $D_m = [D_m^{(ab)}D_m^{(c)}]^{1/2}$.

Equation (2) was used to describe the observations of figure 2. We focus here on the most resistive film for which the theory describes well all anomalous features of the observed dependence of $H_{c2}(T)$, including the upward curvature and the marked increase of $H_{c2}(T)$ at low temperatures. The good agreement between the theory and experiment not only gives one more argument for the two-gap scenario in MgB_2, but also suggests a new way to increase H_{c2} by manipulation of the diffusivity ratio D_σ/D_π using selective atomic substitutions on either Mg or B sites. Both the ratio D_σ/D_π and the anisotropy parameter $D_m^{(ab)}/D_m^{(c)}$ for this dirty film can be extracted from the fit shown in figure 2, giving $D_\pi^{(ab)} \approx 0.12 D_\sigma^{(ab)}$ for $\mathbf{H} \perp ab$ and $[D_\pi^{(ab)}D_\pi^{(c)}]^{1/2} \approx 0.2[D_\sigma^{(ab)}D_\sigma^{(c)}]^{1/2}$ for $\mathbf{H} \parallel ab$. This relation $D_\pi^{(ab)} \sim 0.1 D_\sigma^{(ab)}$ indicates that the π scattering in the dirty film is much stronger than the σ scattering. Thus, according to equations (3) and (4), the slope of $H_{c2}(T)$ near T_c is determined by the σ scattering most likely due to impurities or disorder on B sites, whereas the additional increase of H_{c2} at $T \ll T_c$ results from the predominantly π scattering on Mg sites.

3.2. H_{c2} anisotropy

As follows from figure 2, the shape of the $H_{c2}(T)$ curves change as **H** rotates from $\mathbf{H} \perp ab$ to $\mathbf{H} \parallel ab$. This behaviour, inconsistent with the one-gap Ginzburg–Landau theory, is described well by equations (2) and (5), in which the orientational dependence of H_{c2} is mostly controlled by the anisotropic diffusivity $D_\sigma(\theta)$ for the σ band. For the dirty film, the fit described above gives $D_\pi^{(ab)} \approx 0.12 D_\sigma^{(ab)}$ for $\mathbf{H} \perp ab$ and $[D_\pi^{(ab)}D_\pi^{(c)}]^{1/2} \approx 0.2[D_\sigma^{(ab)}D_\sigma^{(c)}]^{1/2}$ for $\mathbf{H} \parallel ab$, whence we obtain $D_\sigma^{(ab)}/D_\sigma^{(c)} \approx 3D_\pi^{(ab)}/D_\pi^{(c)}$. Thus, the diffusivity for the σ band is more anisotropic than the diffusivity for the 3D π band, in qualitative agreement with *ab initio* calculations [16, 17, 39, 40] and STM measurements [18], which do show a weaker tunnelling probability to the σ band along the c axis. For instance, *ab initio* calculations for clean MgB_2 single crystals [39, 40] have shown that the ratio of the averaged squared Fermi velocities, $\langle v_{ab}^2\rangle_\sigma/\langle v_c^2\rangle_\sigma \approx 46$, for the σ band is much higher than $\langle v_{ab}^2\rangle_\pi/\langle v_c^2\rangle_\pi \approx 0.79$ for the nearly isotropic π band. However, the ratio $D_\sigma^{(ab)}/D_\sigma^{(c)} \approx 3\langle v_c^2\rangle_\pi/\langle v_{ab}^2\rangle_\pi \approx 3.8$ extracted for our dirty film is significantly smaller than the rough estimate $D_\sigma^{(ab)}/D_\sigma^{(c)} \sim \langle v_{ab}^2\rangle_\sigma/\langle v_c^2\rangle_\sigma$ obtained for the simplest point-like isotropic impurity scattering in the Born approximation [36]. There are several factors which may account for this discrepancy. First of all, strong scattering on the actual defect structure in dirty MgB_2 can reduce the anisotropy of the σ band compared to single crystals. For instance, it can be due to the significant buckling of the boron planes observed by TEM on our dirty films (see below). Such buckling increases both the out-of-plane electron scattering and the σ–π band hybridization, reducing the initial anisotropy of the σ band in the dirty film. In addition, a weak c-axis grain misalignment can also contribute to the reduced value of $D_\sigma^{(ab)}/D_\sigma^{(c)}$ in our films. In any case, the simple estimate $D_\sigma^{(ab)}/D_\sigma^{(c)} \sim \langle v_a^2\rangle_\sigma/\langle v_c^2\rangle_\sigma$ should hardly be used for any quantitative conclusions. In fact, no *ab initio* calculations of the anisotropic diffusivities in the σ band have been done yet, so the actual ratio $D_\sigma^{(ab)}/D_\sigma^{(c)}$ for the realistic Fermi surface of MgB_2 and the finite range impurity potential, which accounts for the effects of anisotropic electron screening, remains unknown.

The temperature dependence of the anisotropy parameter $H_{c2}^{||}/H_{c2}^{\perp}$ extracted from the data in figure 2 for both the high-resistivity and epitaxial films is shown in figure 4. As T decreases, the ratio $H_{c2}^{||}/H_{c2}^{\perp}$ in both cases *decreases*, from $\approx$2 at T_c down to $\approx$1.5 at 0 K. This behaviour is opposite to the usual temperature dependence of $H_{c2}(T)$ in MgB_2 single crystals, for which the anisotropy parameter $\gamma(T) = H_{c2}^{||}/H_{c2}^{\perp}$ typically *increases* from $\approx$3 at T_c up to 5–6 at 0 K [8–12]. This unusual dependence of $\gamma(T)$ for the dirty film is due to the large difference between σ and π electron diffusivities ($D_\pi \sim 0.1 D_\sigma$). As a result, the anisotropy parameter $\gamma(T)$ near T_c is determined by a cleaner, more anisotropic 2D σ band. However, at low temperatures the anisotropy of H_{c2} decreases because $\gamma(T)$ is mostly determined by the dirtier 3D π band. Thus, the theory based on equations (2)–(5) does explain the observed decrease of the anisotropy ratio $H_{c2}^{||}/H_{c2}^{\perp}$ as T decreases. The anomalous temperature dependence of $H_{c2}^{||}/H_{c2}^{\perp}$ is one more manifestation of the two-gap superconductivity in MgB_2. Interestingly, the much less resistive epitaxial film exhibits an anisotropy parameter $\gamma(T)$ much smaller than that of single crystals, the temperature dependence of $\gamma(T)$ being nearly constant. The latter is consistent with the dirty-limit theory [36] with the diffusivity

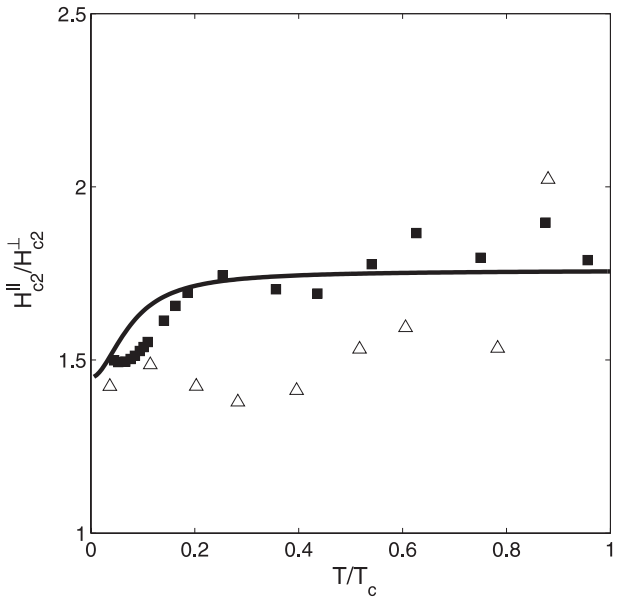

Figure 4. Temperature dependence of the anisotropy parameter $H_{c2}^{\parallel}/H_{c2}^{\perp}$ for the 220 $\mu\Omega$ cm dirty MgB_2 film (full squares) and 7 $\mu\Omega$ cm epitaxial film (open triangles) obtained from the data presented in figure 2. The full curve is calculated from equations (2) and (5) for $D_{\pi}^{(ab)} = 0.09 D_{\sigma}^{(ab)}$ and $D_{\sigma}^{(ab)} = 3 D_{\sigma}^{(c)}$.

ratio $D_{\pi}/D_{\sigma} \sim 0.2$, although the resistivity of the epitaxial film may not be high enough to be in the true dirty limit.

3.3. Impurity scattering mechanisms

At present the mechanisms of impurity scattering in alloyed MgB_2 and its complex substitutional chemistry [12, 41] are not well understood, though we do know that the previously studied [31] quarter of our dirty 220 $\mu\Omega$ cm film was oxygen-rich and had a Mg:B:O ratio of 1:0.9:0.7, as measured by wavelength dispersive spectroscopy [34]. Both O and C, which substitute for B, can result in strong σ scattering [23]. A further insight can be inferred from the electron micrographs presented in figures 5(a) and (b), which show the 'brick-wall' grain nanostructure of this film, which stands in stark contrast to the structure of the lower resistivity epitaxial film [32], which has an almost perfect layered atomic structure, as shown in figure 5(c). In contrast, the dirty film has a 10–20 nm MgB_2 grain size and about 20% of MgO particles of a similar size, which produce much distortion of the atomic packing and thus causes significant scattering in both σ and π bands. Another important feature of the dirty film shown in figure 5(b) is a pronounced buckling of the Mg planes along the c axis, which manifests itself both in variations of the Mg–B spacing and in the intensity of Mg spots. The Mg-plane buckling certainly gives rise to strong *out-of-plane* π scattering, which may explain the relation $D_{\pi}^{(ab)} \sim 0.1 D_{\sigma}^{(ab)}$ obtained from the fit in figure 2.

In the above analysis of the H_{c2} data we assumed that elastic scattering by point defects (nonmagnetic impurities) is the dominant mechanism of the residual resistivity ρ. In this case ρ can be expressed in terms of the diffusivities D_{σ} and D_{π} by

$$1/\rho = e^2(N_{\sigma} D_{\sigma} + N_{\pi} D_{\pi}), \qquad (6)$$

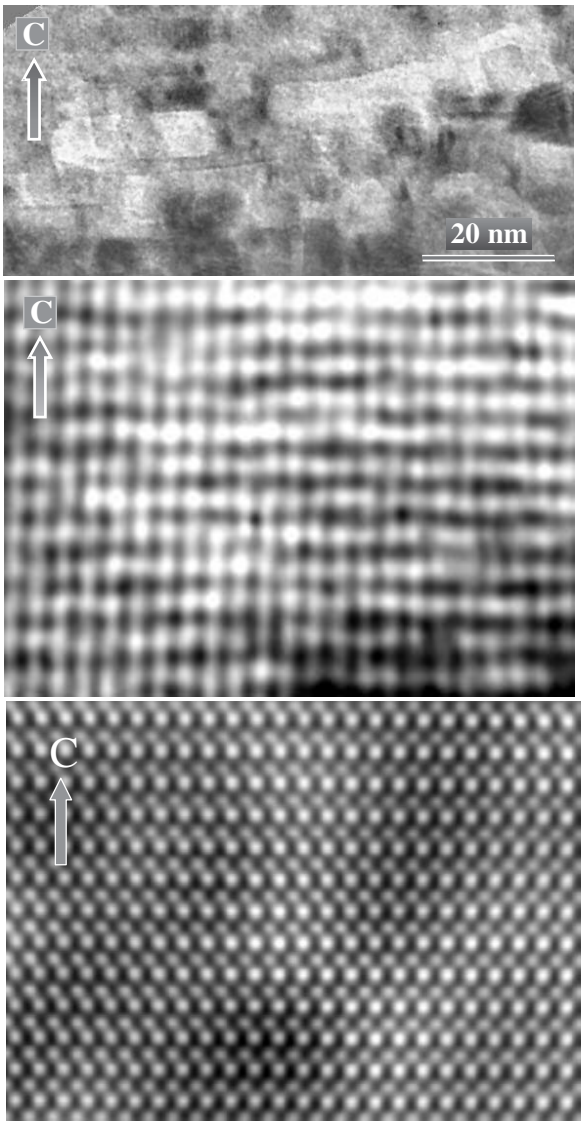

Figure 5. Transmission electron micrographs of the two films. (a) High resistivity film ($\rho(40\ \mathrm{K}) = 220\ \mu\Omega$ cm), showing a c-axis textured 'brick-wall' structure with imperfectly distinguished MgB_2 and MgO grains with characteristic sizes of 10–20 nm. (b) Atomic resolution image showing the highly strained and buckled Mg structure, especially along the c axis. The variable intensity of the Mg bright spots indicates buckling of the Mg rows in the direction perpendicular to the plane of the figure. (c) More-perfect structure of the epitaxial film showing much less evidence for distortion in this low resistivity film ($\rho(40\ \mathrm{K}) = 7\ \mu\Omega$ cm).

where N_{σ} and N_{π} are partial densities of states in the σ and π bands, respectively, e is the electron charge and the weak interband scattering is neglected. Using equations (3) and (6), D_{σ} and D_{π} can be extracted from the observed ρ and H'_{c2} at T_c [36]. However, in addition to impurity scattering, the resistivity of real MgB_2 samples can also be strongly affected by extrinsic mechanisms, such as scattering on grain boundaries or second phase nanoprecipitates, which effectively reduce the current-carrying cross section [42]. While it is not easy to unambiguously separate extrinsic and intrinsic contributions to ρ, we can nevertheless make qualitative conclusions about the scattering mechanisms by analysing *both* H_{c2} and ρ data. Indeed, H_{c2} can only be affected by

disorder on a scale shorter than the clean limit GL coherence length, $\xi_\sigma(0) = [\phi_0/2\pi H_{c2}(0)]^{1/2}$, which is about 8–10 nm for the values of $H_{c2}(0) \approx 3.5$–5 T characteristic of single crystals [8–12]. Therefore, the fact that H_{c2} of the dirty film is increased by almost ten times compared to single crystals does indicate strong scattering on the atomic scale $\ll$10 nm, most likely due to impurities, especially O and C, on the B and Mg planes and quenched crystalline disorder and buckling of Mg planes, as discussed above. In turn, direct electron scattering from the grain structure on the scale 10–20 nm $> \xi_\sigma(0)$, clearly seen in figure 5(a), may not be the primary reason for the observed H_{c2} enhancement, although additional scattering on grain boundaries and MgO precipitates can certainly increase the global resistivity. However, significant local strains produced by the nanoprecipitates and grain boundary structure might cause lattice buckling on the atomic scale, in which case grain boundaries could indirectly contribute to the H_{c2} enhancement.

Our data clearly show the decisive qualitative effect of resistivity on H_{c2}. However, the extrinsic mechanisms [42] may be indeed very important for understanding why H_{c2}, even in dirty MgB_2 samples, does not always scale with ρ and why samples with comparable H_{c2} can have very different ρ. For instance, our dirty 220 $\mu\Omega$ cm film has nearly the same slope H'_{c2} at T_c as the 18 $\mu\Omega$ cm Mg-annealled polycrystal. We can therefore conclude that scattering on the nanoscale grain boundary structure shown in figure 5 could indeed cause a significant extrinsic contribution ρ_{ex} to the overall resistivity ρ. To account for ρ_{ex} in the above dirty-limit theory, one should substitute only the impurity part, $\rho - \rho_{ex}$, instead of ρ in equation (6), which determines the electron diffusivities D_σ and D_π. Since the extrinsic mechanisms do not affect H_{c2}, they do not change the results of our analysis based on equations (2)–(6).

In principle, the contribution of ρ_{ex} to the total resistivity ρ could be extracted from the measured $\rho(T_c)$ and the $H_{c2}(T)$ curve with the use of equations (2) and (6). First, from the fit to the $H_{c2}(T)$ curve, one can evaluate the values of D_σ and D_π, using the coupling constants λ_{mn} and the partial densities of states N_σ and N_π from *ab initio* calculations [16, 17, 38] as input parameters in equation (2). Next, the impurity contribution ρ_i can be calculated upon substitution of the so-obtained D_σ and D_π into equation (6), giving the extrinsic contribution, $\rho_{ex} = \rho - \rho_i$.

3.4. MgB_2 as an emerging high-field conductor material

The observed significant enhancement of $H_{c2}(T)$, both for bulk samples and especially for the high-resistivity thin film, may provide the missing component for the other essentials needed for a viable MgB_2 conductor technology. Low raw material cost, round wire capability, high critical current densities and irreversibility fields are all possessed by MgB_2 today [6]. Our results show that the two-band physics of dirty MgB_2 provides a new way to boost H_{c2} at low temperatures, so that it betters all low-T_c superconductors except $PbMo_6S_8$, for which $H_{c2}(0) = 59$ T, as shown in figure 6. Since no viable wire route has ever been developed for $PbMo_6S_8$, the real competitors to MgB_2 are only HTS tapes of $Bi_2Sr_2CaCu_2O_{8-x}$, $(Bi, Pb)_2Sr_2Ca_2Cu_3O_{10-x}$, $YBa_2Cu_3O_{7-\delta}$, Nb_3Sn or Nb–Ti [3]. As follows from figure 6, MgB_2 is already competitive

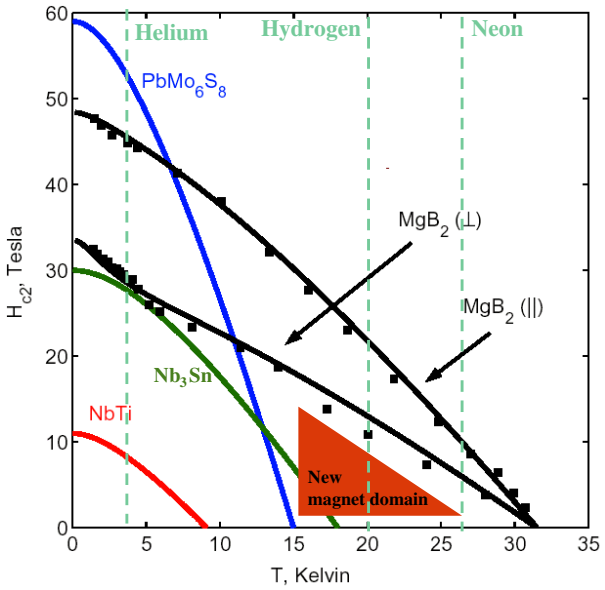

Figure 6. Comparison of upper critical fields of low-T_c superconductors. Here we show $H_{c2}(T)$ curves for Nb–Ti, high-field Nb_3Sn, high resistivity MgB_2 films from this work and $PbMo_6S_8$, which has the highest H_{c2} for non-cuprate superconductors. The high field performance of MgB_2 is superior to that of Nb_3Sn both for parallel and perpendicular fields. The marked area shows the temperature and field range where the 'medium temperature' superconducting applications may be most effective [14]. The vertical broken lines show 1 atm boiling points of different cryogenic coolants.

(This figure is in colour only in the electronic version)

with Nb_3Sn at low temperatures and with cuprate HTS at 20–25 K for electrical utility applications for which fields up to $\sim$5 T are needed [13]. Today the majority of superconducting magnet applications use Nb–Ti at 4.2 K and fields below 7 T. This field capability is now open to MgB_2 at much higher temperatures (15–25 K) accessible to cryocoolers where the wide stability margin of MgB_2 can offer clear advantages over all Nb-based superconductors [14].

One important path for making suitable MgB_2 conductors is based on the powder-in-tube (PIT) route to produce both round wires and tapes [6]. This process has been validated by the production of high-performance, round PIT Nb_3Sn wires, which typically have several hundreds of 20–50 μm filaments with low hysteretic loss [43]. Although tape-like HTS conductors are commercially available, they have relatively high ac losses and cannot easily be cabled to make conductors of arbitrary amperage. In contrast, MgB_2 offers the advantages of round-wire geometry, low raw materials cost, high strength, the capability of being fabricated by a proven wire technology coupled with high J_c and moderate H_{c2} anisotropy. As we show in this paper, strong π scattering due to disorder in the Mg sublattice can significantly boost the upper critical field at low temperatures without great penalty to T_c. Another important result is that introducing strong scattering in the π band by alloying the Mg sublattice can significantly reduce the H_{c2} anisotropy, compared to MgB_2 single crystals (see figure 4). We believe that the peculiar high-field behaviour of our samples and their good description by a theory of dirty two-gap superconductivity clearly show

the general trend for further H_{c2} enhancement in MgB_2. Therefore, further systematic studies of the unexplored physics and materials science of MgB_2 alloys combined with high-field H_{c2} and J_c measurements would be invaluable both for a better understanding of high-field superconductivity in MgB_2 and for future magnet applications.

The results of this work also pose a fundamental question: how far can alloying further increase H_{c2} of MgB_2? As we have shown both experimentally and theoretically, the two-band physics does remove one essential obstacle for higher H_{c2} at low T due to replacing the factor of 0.69 in equation (1) by a function $\chi(D_\sigma, D_\pi)$, which can be *greater than 1*. As a result, much higher $H_{c2}(0)$ values are possible for a given slope H'_{c2} at T_c. To properly understand what further improvements in properties can be derived by alloying MgB_2, it is vital to measure the whole $H_{c2}(T)$ curve over a wide range of T and ρ, so that the peculiar alloying potential of this apparently simple material with complex substitutional chemistry [41] can be understood. For instance, for dirty MgB_2 with values of $H'_{c2} = 1$ T K^{-1}, $T_c = 40$ K and $\chi = 1$, the theory predicts $H_{c2}(0) = 40$ T. Such a high $H_{c2}(0)$ already greatly exceeds $H_{c2}(0)$ for Nb_3Sn, even though H'_{c2} is still significantly smaller than the 2 T K^{-1} characteristic of other LTS and HTS, not to mention $\sim$2.5 T K^{-1} for $PbMo_6S_8$ (see figure 6). For $H'_{c2} = 1$ T K^{-1}, the shortest GL *in-plane* coherence length $\xi_\sigma(0) = [\phi_0/2\pi T_c H'_{c2}]^{1/2} \approx 3$ nm for the σ band is still large enough to ensure no significant magnetic granularity and weak link behaviour at grain boundaries. Thus, there are no inherent limitations to a further increase of H'_{c2} toward the HTS, Nb–Ti and Nb_3Sn levels of 2 T K^{-1} by proper alloying with nonmagnetic impurities or by quenched-in lattice disorder in MgB_2. For $H'_{c2} \approx 2$ T K^{-1} the field $H_{c2}(0)$ would approach the paramagnetic limit of $\sim$70 T for MgB_2, in which case strong coupling and spin effects should be included in a more general theory based on the Eliashberg equations [17, 38].

Acknowledgments

We have greatly benefited from discussions and assistance from P Manfrinetti, A Palenzona, M Rzchowski, A Godeke, B Senkowicz, P Voyles, L Balicas, A Lacerda and G Boebinger. The work was primarily supported through the NSF Nanostructured Materials and Interfaces Materials Research Science and Engineering Center at the University of Wisconsin.

References

[1] Nagamatsu J, Nakagawa N, Muranaka T, Zenitani Y and Akimitsu J 2001 Superconductivity at 39 K in magnesium diboride *Nature* **410** 63–4
[2] Canfield P C and Crabtree G W 2003 Magnesium diboride: better late than never *Phys. Today* **56** 34–40
[3] Dou S X *et al* 2002 Enhancement of the critical current density and flux pinning of MgB_2 by nanoparticle SiC doping *Appl. Phys. Lett.* **81** 3419–21
[4] Wang J *et al* 2002 High critical current density and improved irreversibility field in bulk MgB_2 made by a scalable, nanoparticle addition route *Appl. Phys. Lett.* **81** 2026–8
[5] Komori K *et al* 2002 Approach for the fabrication of MgB_2 superconducting tape with large in-field transport critical current density *Appl. Phys. Lett.* **81** 1047
[6] Flukiger R, Suo H L, Musolino N, Beneduce C, Toulemonde P and Lezza P 2003 Superconducting properties of MgB_2 tapes and wires *Physica* C **385** 286–305
[7] Larbalestier D C *et al* 2001 Strongly linked current flow in polycrystalline forms of the new superconductor MgB_2 *Nature* **410** 186–9
[8] Angst M, Puzniak R, Wisniewski A, Jun J, Kazakov S M, Karpinski J, Roos J and Keller H 2002 Temperature and field dependence of anisotropy of MgB_2 *Phys. Rev. Lett.* **88** 1670041–4
[9] Perkins G K *et al* 2002 Superconducting critical fields and anisotropy of a MgB_2 single crystal *Supercond. Sci. Technol.* **15** 1156–9
[10] Sologubenko A V, Jun J, Kazakov S M, Karpinski J and Ott H R 2002 Temperature dependence and anisotropy of the upper critical field of MgB_2 *Phys. Rev.* B **65** 180505-1–4
[11] Zehetmayer M *et al* 2002 Mixed state properties of superconducting MgB_2 single crystals *Phys. Rev.* B **66** 0525051–4
[12] Canfield P C, Bud'ko S L and Finnemore D K 2003 An overview of the basic physical properties of MgB_2 *Physica* C **385** 1–7
[13] Larbalestier D, Gurevich A, Feldmann D M and Polyanskii A 2001 High transition temperature superconducting materials for electric power applications *Nature* **414** 368–77
[14] Schultz J H 2003 The medium temperature superconductor (MTS) design philosophy *IEEE Trans. Appl. Supercond.* **13** 1604–7
[15] Grant P 2001 Rehearsals for prime time *Nature* **411** 532–3
[16] Liu A Y, Mazin I I and Kortus J 2001 Beyond Eliashberg superconductivity in MgB_2: anharmonicity, two-phonon scattering and multiple gaps *Phys. Rev. Lett.* **87** 0870051–4
[17] Choi H J, Roundy D, Sun H, Cohen M L and Loule S G 2002 The origin of anomalous superconducting properties of MgB_2 *Nature* **418** 758–60
[18] Iavarone M *et al* 2002 Two-band superconductivity in MgB_2 *Phys. Rev. Lett.* **89** 1870021–4
[19] Schmidt H, Zasadzinski J E, Gray K E and Hinks D G 2002 Evidence for two-band superconductivity from break-junction tunneling in MgB_2 *Phys. Rev. Lett.* **88** 1270021–4
[20] Chen X K, Kostantinovic M J, Irwin J C, Lawrie D D and Franck J P 2001 Evidence for two gap superconductivity in MgB_2 *Phys. Rev. Lett.* **87** 1570021–4
[21] Bouquet F, Wang Y, Sheikin I, Plackowski T, Junod A, Lee S and Tajima S 2002 Specific heat of single crystal MgB_2: a two-band superconductor with different anisotropies *Phys. Rev. Lett.* **89** 257001–4
[22] Cubitt R, Levett S, Bud'ko S L, Anderson N E and Canfield P C 2003 Experimental evidence for anisotropic double gap behavior in MgB_2 *Phys. Rev. Lett.* **90** 1570021–4
[23] Mazin I I *et al* 2002 Superconductivity in MgB_2: clean or dirty? *Phys. Rev. Lett.* **89** 1070021–4
[24] Fietz W A and Webb W W 1967 Magnetic properties of some type II superconductors near the upper critical field *Phys. Rev.* **161** 423–33
[25] Orlando T P, McNiff E J, Foner S and Beasley M R 1979 Critical fields, Pauli paramagnetic limiting, and material parameters of Nb_3Sn and V_3Si *Phys. Rev.* B **19** 4545–61
[26] Ketterson J B and Song S N 1999 *Superconductivity* (Cambridge: Cambridge University Press)
[27] Patnaik S *et al* 2001 Electronic anisotropy, magnetic field–temperature phase diagram and their dependence on resistivity in *c*-axis oriented MgB_2 thin films *Supercond. Sci. Technol.* **14** 315–9
[28] Gumbel A *et al* 2002 Improved superconducting properties in nanocrystalline bulk MgB_2 *Appl. Phys. Lett.* **80** 2725–8

[29] Bugoslavsky Y *et al* 2001 Enhancement of high-field critical current density of superconducting MgB_2 by proton irradiation *Nature* **411** 561–3
[30] Bouquet F *et al* 2003 Unusual effects of anisotropy on the specific heat of ceramic and single crystal MgB_2 *Physica* C **385** 192–204
[31] Eom C B *et al* 2001 Thin film magnesium boride superconductor with very high critical current density and enhanced irreversibility field *Nature* **411** 558–60
[32] Bu S D *et al* 2002 Synthesis and properties of *c*-axis oriented MgB_2 epitaxial films *Appl. Phys. Lett.* **81** 1851–3
[33] Braccini V *et al* 2002 Significant enhancement of irreversibility field in clean-limit bulk MgB_2 *Appl. Phys. Lett.* **81** 4577–9
[34] Song X *et al* 2002 Anisotropic grain morphology, crystallographic texture and their implications for flux pinning in MgB_2 pellets, filaments and thin films *Supercond. Sci. Technol.* **15** 511–8
[35] Ando Y *et al* 1999 Resistive upper critical fields and irreversibility lines of optimally doped high-T_c cuprates *Phys. Rev.* B **60** 12475–9
[36] Gurevich A 2003 Enhancement of H_{c2} by nonmagnetic impurities in dirty two-gap superconductors *Phys. Rev.* B **67** 1845151–13
[37] Koshelev A E and Golubov A A 2003 Mixed state in a dirty two-band superconductor: application to MgB_2 *Phys. Rev. Lett.* **90** 1770021–4
[38] Golubov A A *et al* 2002 Specific heat of MgB_2 in a one- and a two-band model from first-principle calculations *J. Phys.: Condens. Matter* **14** 1353–60
[39] Belashchenko K D, van Schilfgaarde M and Antropov V P 2001 Coexistence of covalent and metallic bonding in the boron intercalation superconductor MgB_2 *Phys. Rev.* B **46** 0925031–4
[40] An J M and Pickett W E 2001 Superconductivity in MgB_2: covalent bonds driven metallic *Phys. Rev. Lett.* **86** 4366–9
[41] Cava R J, Zandbergen H W and Inumaru K 2003 The substitutional chemistry of MgB_2 *Physica* C **385** 8–15
[42] Rowell J M 2003 The widely variable resistivity of MgB_2 samples *Supercond. Sci. Technol.* **16** R17–27
[43] Lindenhovius J, Hornsveld E, den Ouden A, Wessel W and ten Kate H 2000 Powder-in-tube (PIT) Nb_3Sn conductors for high field magnets *IEEE Trans. Appl. Supercond.* **10** 975–8